

Review on critical impact velocities in tension and shear

J.R. Klepaczko

Metz University, Laboratory of Physics and Mechanics of Materials, UMR-CNRS 7554, Ile du Sauley, F-57045 Metz, Cedex 01, France

Received 22 September 2004; received in revised form 23 August 2005; accepted 24 August 2005
Available online 24 October 2005

Abstract

Adiabatic heating, due to conversion of plastic work into thermal energy, substantially changes the boundary value problems in the theory of plastic wave propagation. Besides a systematic review of the subject, the thermal coupling during plastic wave propagation leading to adiabatic wave trapping is the main subject of this study. Two cases are analyzed, the adiabatic wave trapping in tension and also in shear. The case of shear is relatively new. The wave trapping by adiabatic deformation via thermal softening leads to the so called critical impact velocity (CIV). Theory, experiments and numerical analyses of the CIV in tension and shear is the main part of this paper.

© 2005 Elsevier Ltd. All rights reserved.

Keywords: Critical impact velocity; Dynamic plasticity; Thermal coupling; Impact shearing

1. Introduction

In the late 1940s of the last century von Kármán [1–4] and others developed a theory for propagation of one-dimensional plastic waves in a long bar. It was then demonstrated that if an infinite bar is loaded in tension by a sufficiently high impact velocity, plastic deformation is concentrated near the impact end of the bar. The theory was limited to rate independent and isothermal case. However, plastic deformation of materials is rate and temperature dependent. In this paper a more detailed discussion is offered on theory of plastic wave propagation with thermal coupling. The adiabatic heating causes usually a material softening leading to adiabatic wave trapping. Localization of plastic deformation in adiabatic conditions superimposed on inertia effects (waves) causes that the plastic wave speed reaches zero and the critical impact velocity (CIV) occurs. It is shown that the CIV can be observed in both tension and shear. The case of shear has been found and analyzed more recently [5–10].

2. Isothermal propagation of plastic waves (revisited)

Although elastic waves were studied since the beginning of Nineteenth Century, for example T. Young in 1807 studied the propagation of elastic strains in a cylindrical bar subjected to tension impact. The theory of plastic waves was formulated in the mid of Twentieth Century by von Kármán and Taylor, [1,3,4]. The unloading

E-mail address: klepaczko@lpmm.sciences.univ-metz.fr.

elastic waves were introduced by Rakhmatulin [11]. The stress waves caused by an impact at the end of a semi-infinite bar has been analyzed in the case where the impact velocity is high enough to produce plastic deformation.

Consider a bar extending from $x_1 = -\infty$ to $x = 0$ and assume that the end at $x = 0$ is loaded by impact with a constant velocity V_0 . The stress–strain relation for the material is given in the form $\sigma(\varepsilon)$, where σ and ε are, respectively, the stress and strain. The $\sigma(\varepsilon)$ relation is unique and has a smooth first derivative $d\sigma/d\varepsilon$ in the form of decreasing function of strain. Such assumption leads to the so-called rate-independent theory of plastic wave propagation. It means that initially the rate effects are neglected. However, in the up-to-date approach the existence is accepted of *one and only one* stress–strain relation which may be also a high-strain rate relation at strain rate say 10^3 s^{-1} . In addition, the radial contraction of the material, that is contribution of the radial velocity to the inertia effects is neglected. Under these assumptions, the equation of motion for an element of a slender bar can be written in the form

$$\frac{\partial^2 U_1}{\partial t^2} = C^2(\varepsilon) \frac{\partial^2 U_1}{\partial x_1^2} \quad \text{and} \quad \varepsilon = \varepsilon_e + \varepsilon_p \tag{1}$$

in the elastic range $C_0 = (E/\rho)^{1/2}$ and in the plastic range $C_p(\varepsilon_p) = (1 \, d\sigma/\rho \, d\varepsilon_p)^{1/2}$. The waves propagate in the x_1 direction, U_1 is the displacement in that direction, t is time, C_0 is the longitudinal elastic wave speed in slender rods, and $C_p(\varepsilon_p)$ is the plastic wave speed as a decreasing function of plastic strain ε_p . In the elastic range the wave speed is constant, it depends only on the density ρ and Young’s modulus E . Since the boundary conditions are $U_1 = V_0 t$ for $x_1 = 0$ and $U_1 = 0$ for $x_1 = -\infty$ the solution of Eq. (1) is in the form

$$U_1(x_1, t) = V_0 \left[t + \left(\frac{x_1}{C_p(\varepsilon_p)} \right) \right]. \tag{2}$$

The plastic wave speed has an arbitrary value. The second solution is obtained by putting

$$\left(\frac{d\sigma}{\rho \, d\varepsilon_p} \right)^{1/2} = \pm \frac{x_1}{t} \quad \text{or} \quad C_p(\varepsilon_p) = \pm \frac{x_1}{t}. \tag{3}$$

In the above analysis presented previously in [1,4] a special case is considered in which the plastic strain is a function of x_1/t but not of x_1 and t independently.

Since Eq. (1) is a quasi-linear differential equation of the second order, and of the type of the wave equation, it can be also solved by the method of characteristics [12]. The definition of the characteristic line is (x_1 is replaced by x)

$$\frac{dx}{dt} = \pm C(\varepsilon) \tag{4}$$

in the elastic range $dx/dt = \pm C_0$ and in the plastic range $dx/dt = \pm C_p(\varepsilon_p)$. The partial differential equation (1) satisfied along the characteristic lines due to consistency conditions is

$$dv = \pm C(\varepsilon) \, d\varepsilon. \tag{5}$$

Along two sets of characteristics the mass velocities in both elastic and plastic ranges are given by

$$v = \pm C_0 \varepsilon \quad \text{and} \quad v(\varepsilon_p) = \pm \int_0^{\varepsilon_p} C_p(\xi) \, d\xi. \tag{6}$$

The first relation in (6) occurs along the linear characteristics $dx/dt = \pm C_0$. The mass velocity $v(\varepsilon_p)$ defined by the second relation in (6), that is in the plastic range, occurs along non-linear characteristics $dx/dt = \pm C_p(\varepsilon_p)$. In a more general approach, applied nowadays, the stress–strain relation is assumed at constant strain rate, typical value $\sim 10^3 \text{ s}^{-1}$, and the temperature is assumed as the initial temperature. The generalized wave speed is given by

$$C_p(\varepsilon_p) = \pm \left(\frac{1 \, d\sigma}{\rho \, d\varepsilon_p} \right)_{\dot{\varepsilon}, T}^{1/2}. \tag{7}$$

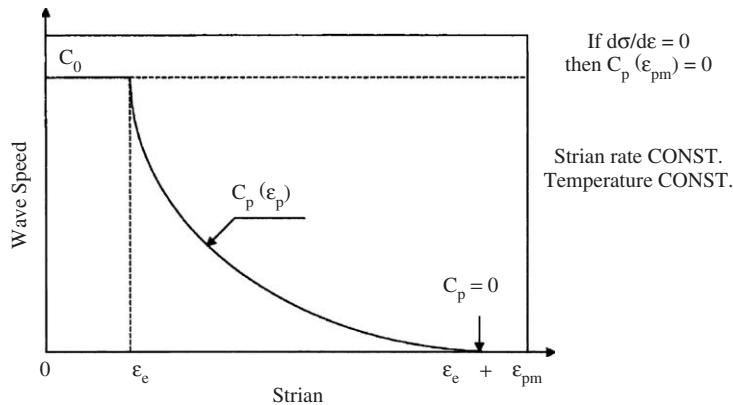


Fig. 1. Schematic changes of the wave speeds as a function of total strain (elastic plus plastic), ϵ_e is the strain of elastic limit, ϵ_{pm} is the limiting case when $d\sigma/d\epsilon = 0$ and then $C_p = 0$.

Schematic variation of the elastic and plastic wave speed as a function of the total strain is shown in Fig. 1. Thus, the strain rate and temperature are parameters, not variables, in the “rate independent” Kármán–Taylor–Rakhmatulin theory (KTR). Although the rate-dependent theory of plastic wave propagation is well developed, it can be shown that KTR approximation is quite good.

3. Early experiments on impact tension and plastic wave propagation

A trivial statement seems to be obvious: impact testing of materials is different than quasi-static testing, or standard testing. This statement is true for all types of tests, including tension, compression and shear or torsion. In impact testing two additional effects must be taken into account: wave propagation (elastic and plastic) and thermal coupling due to adiabatic heating, that is conversion of the plastic work into heat. The wave propagation causes stress and strain gradients in specimens. This is a source of size effects in impact testing of materials. A long specimen will behave differently than a short one. The thermal coupling causes acceleration of all kinds of instabilities in plastic flow, for example adiabatic shear bands (ASB) in shear or torsion tests. Those two factors impose limits in materials testing at high strain rates, specially when one attempts to obtain mechanical properties in the “elementary volume” and transmit this information into a constitutive relation.

One of the earliest report on tension impact test is that of Mann (1936), [13]. Experiments were carried out at the Watertown Arsenal Laboratory (USA) using a specially built rotational hammer. This apparatus was capable producing impact velocities up to 1000 ft/s (~ 300 m/s). The effect of impact velocity on the failure energy was reported for several materials including SAE 1035 steel. It was found that independently of the specimen length the maximum of failure energy occurred at specific well defined impact velocity. This was the first report on the CIV. Development of the KTR theory of wave propagation caused further experimental work on the effect of impact velocity on permanent strain distribution along specimen and failure. Since all specimens are of finite length, some reflections of elastic and plastic waves from the fixed end amplifies further the strain gradients along a specimen. For example, Fig. 2 shows distributions of plastic strain after failure of 40 in (~ 1016 mm) specimen, curve A, for annealed aluminum at impact velocity 80 ft/s (24.4 m/s), [2]. Because of relatively long specimen the effect of wave reflections from the fixed end is well visible. Because the impact velocity was not so high the CIV does not appear. Two theoretical analyses by the KTR theory are shown in this figure, the first one with no wave reflection, curve B, and the second with the wave reflections, curve C. A qualitative agreement for the case C is acceptable showing that the KTR theory can account for the main features of plastic wave propagation.

Another experimental proof of the CIV in tension was published in [14]. In that case the failure energy was obtained experimentally for different specimen lengths and impact velocities. The result for SAE 1020 CR steel is reproduced in Fig. 3. This is the 3D surface of the failure energy versus impact velocity up to 200 ft/s

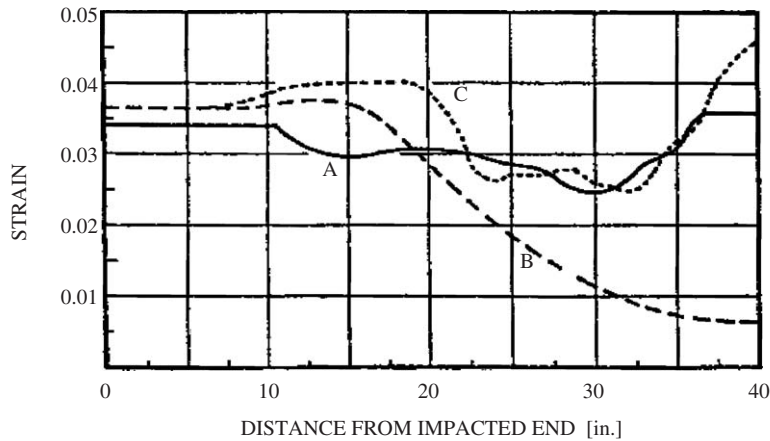


Fig. 2. Strain distributions for annealed aluminum after failure in tension, specimen length 40 in (1016 mm), impact velocity 80 ft/s (24.4 m/s), A—experimental, B—theoretical (KTR) no reflection, C—theoretical (KTR) with reflection [2].

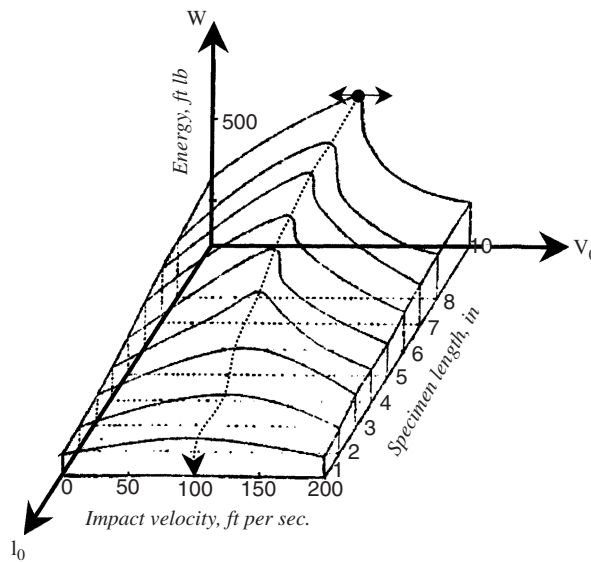


Fig. 3. The effect of specimen length and impact velocity in tension on the failure energy for SAE 1020 Cold Rolled (CR) steel [14].

(61 m/s) and specimen length from 1 in to 10 in (25.4–254 mm). At impact velocities in the neighborhood of 100 ft/s (30.5 m/s) the failure energy reaches maximum for any specimen length. At higher velocities there is a very definite decrease in the energy. The important fact is that the maximums of the failure energy occur independently of the specimen length at the same impact velocity 30.5 m/s.

The concept of the CIV in tension is discussed for the first time by Duwez and Clark [14] from the both points of view: theory and experiment. Those authors stated “There exists a velocity of impact, called the critical velocity, above which rupture will occur near the impacted end of the bar, and the remainder of the bar will be essentially free of plastic deformation”.

Of course, values of CIV in tension for different materials may provide a measure of ductility. Some aspects of ductility related to CIV in tension were discussed in [15]. The CIV in tension was analyzed and confirmed. The CIV was noted to vary considerably for high-speed tensile testing, from 125 ft/s (38.1 m/s) for Mo (0.5% Ti) to 435 ft/s (132.7 m/s) for 17-7 PH stainless steel.

A general conclusion can be reached that there is a speed limit in the dynamic tension test in determination of the material properties, that is stress versus strain, when the quasi-static approach is applied. This limit depends on intrinsic material properties, specimen dimensions and impact velocity. A simple numerical calculations of impact tension was demonstrated in [16] how the “stress–strain” curves in tension degenerate when the impact velocity is increased. A more advanced numerical study of the CIV in tension was reported in [22].

4. The critical impact velocity in tension—isothermal case

The KTR theory of plastic wave propagation offers possibility to estimate values of the CIV in tension for different materials. According to the KTR theory the integral in the form of Eq. (6) defining the mass velocity reaches the maximum at specific strain ε_m . If the wave speed reaches zero at specific total strain ε_m , that is $d\sigma/d\varepsilon = 0$ and $C(\varepsilon_m) = 0$, then the mass velocity reaches its maximum and higher mass velocities cannot propagate. In other words this is theoretical definition of the CIV in tension, $V_0 = v_{cr}$, given by

$$v(\varepsilon_m) = \int_0^{\varepsilon_m} C(\xi) d\xi, \quad \dot{\varepsilon} = \text{const and } T = \text{const.} \quad (8)$$

Value of the CIV is simply the integral of $C(\varepsilon)$ curve shown schematically in Fig. 1. The integral (8) can be split into two parts, the first one over the elastic range, $0 < \varepsilon < \varepsilon_e$, and the second over the plastic range, $\varepsilon_e < \varepsilon < \varepsilon_{pm}$, where ε_e is strain at the yield limit [17]. Thus

$$v_{cr} = \int_0^{\varepsilon_e} C_0 d\varepsilon + \int_{\varepsilon_e}^{\varepsilon_{pm}} C_p(\varepsilon_p) d\varepsilon_p. \quad (9)$$

Since the elastic wave speed in slender rods is assumed constant, $C_0 = \text{const}$, the first part can be integrated, then

$$v_{cr} = C_0 \varepsilon_e + \int_{\varepsilon_e}^{\varepsilon_{pm}} C_p(\varepsilon_p) d\varepsilon_p \quad (10)$$

or in another form, when the yield stress is introduced, $\sigma_e = E\varepsilon_e$,

$$v_{cr} = \frac{\sigma_e}{(E\rho)^{1/2}} + \int_{\varepsilon_e}^{\varepsilon_{pm}} C_p(\varepsilon_p) d\varepsilon_p. \quad (11)$$

Of course, question arises how to define the upper limit of integration ε_{pm} . Many materials show necking before the saturation stress is reached. When necking occurs at specific plastic strain, than ε_{pm} can be assumed as the upper limit of integration in Eqs. (9)–(11). If the Considère's condition of instability is assumed ($d\sigma/d\varepsilon = \sigma$, [18]), and plastic behavior is approximated in quasi-static conditions by $\sigma = B\varepsilon^n$ then $\varepsilon_{pm} = n$. Such the first order approximation yields relatively good, but lower than expected, values of the CIV in tension.

In conclusion the CIV is a function of elastic and plastic properties of materials. For materials with a high yield limit and low rates of strain hardening leading to a small instability strain (necking) the first term in Eqs. (9)–(11) dominates. Whereas for soft materials with a low yield stress and a high strain hardening the second term is more important. Those two terms compensate each other, and values of the CIV do not vary substantially for different engineering materials. Experimentally determined values of the CIV in tension vary from 15 m/s for single crystals up to 230 m/s for Hadfield steel. The last value is expected to be quite high due to martensitic phase transformation (TRIP effect).

5. Theoretical considerations, effect of initial temperature and strain rate

As it is mentioned in the first part of this paper the initial temperature and strain rate, both assumed constant, can be introduced in theoretical considerations as parameters. The only mathematical condition is that the stress versus strain relation must be unique. It was shown on the basis of experiments in [19] for aluminum and copper that plastic waves can propagate relatively small distances and the mean strain rates in

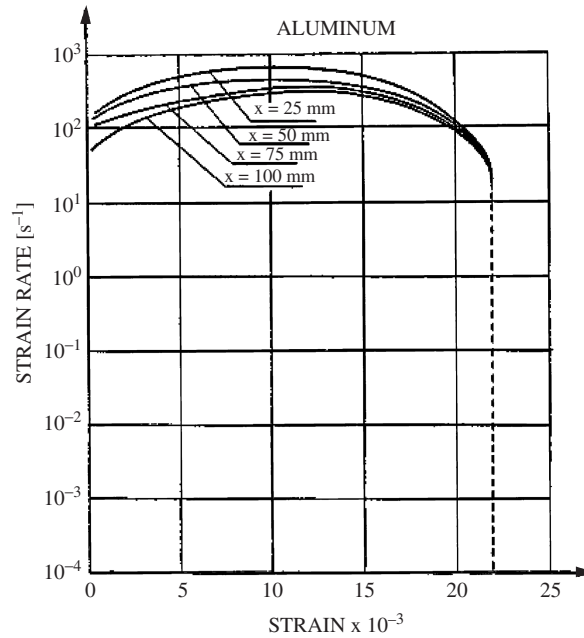


Fig. 4. Logarithmic changes of strain rate in the front of plastic wave at different distances for aluminum versus strain, quasi static strain rate was assumed as 10^{-4} s^{-1} [19].

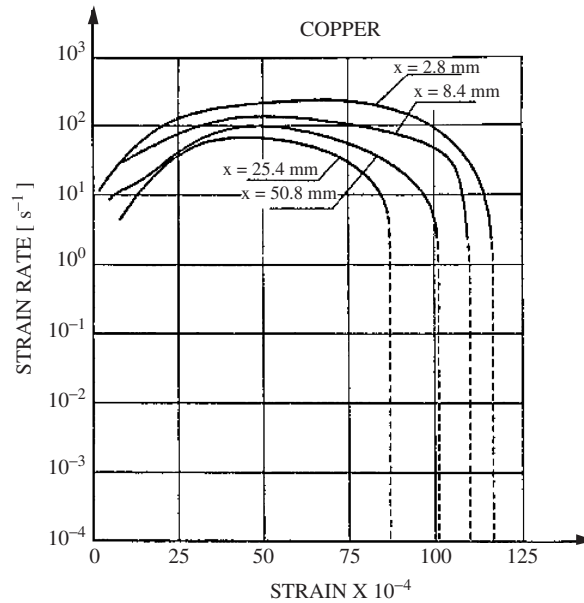


Fig. 5. Logarithmic changes of strain rate in the front of plastic wave at different distances for copper versus strain, quasi static strain rate was assumed as 10^{-4} s^{-1} [19].

the wave front vary from $\sim 10^2 \text{ s}^{-1}$ to $\sim 5 \times 10^2 \text{ s}^{-1}$. Those results are shown in Figs. 4 and 5 as logarithm of strain rate in the wave front versus strain. In the case of the KTR theory the strain rate can be assumed constant at the mean level, for example for aluminum 10^2 s^{-1} and for copper $5 \times 10^2 \text{ s}^{-1}$.

Effects of the initial temperature on CIV are introduced via changes of elastic constants and changes of the flow stress in the plastic range. The elastic wave speed in slender rods can be generalized

as follows:

$$C_0(T) = \left(\frac{E(T)}{\rho(T)} \right)^{1/2}, \quad 0 < \varepsilon < \varepsilon_c. \tag{12}$$

The main effect in changes of C_0 versus temperature lies in changes of elastic properties, changes of the density is the second order contribution. The effect of temperature on Young’s modulus is given by [20]

$$E(T) = E_0 \left\{ 1 - \frac{T}{T_m} \exp \left[\theta * \left(1 - \frac{T_m}{T} \right) \right] \right\}. \tag{13}$$

If $\rho(T) \approx \text{constant}$ then $C_0(T)$ is given by

$$C_0(T) = C_0(0) \left\{ 1 - \frac{T}{T_m} \exp \left[\theta * \left(1 - \frac{T_m}{T} \right) \right] \right\}^{1/2} \quad \text{with} \quad C_0(0) = \pm \left(\frac{E_0}{\rho_0} \right)^{1/2}, \tag{14}$$

where ρ_0 is the density at $T = 0$ and E_0 is the Young’s modulus at $T = 0$ K, T_m is the melting point and $\theta*$ is the characteristic homologous temperature.

Since in this stage of the analysis the temperature is assumed as the initial temperature T_0 the speed of plastic waves will change only in direct relation to changes of the stress–strain relation and its first derivative both as a function of temperature. In order to retain generality the following symbolic constitutive relation is assumed

$$\sigma(\varepsilon_p, \dot{\varepsilon}, T) = f_1(\varepsilon_p) f_2(\dot{\varepsilon}) f_3(T). \tag{15}$$

Such structure of constitutive relations is quite common in many studies on dynamic plasticity. The first derivative and the plastic wave speed are given by

$$\frac{d\sigma}{d\varepsilon_p} = f_2(\dot{\varepsilon}) f_3(T) \frac{df_1}{d\varepsilon_p} \quad \text{and} \quad C_p(\varepsilon_p)_{T,\dot{\varepsilon}} = \pm \left[f_2(\dot{\varepsilon}) f_3(T) \left(\frac{1}{\rho} \frac{df_1}{d\varepsilon_p} \right) \right]^{1/2}. \tag{16}$$

Thus, the CIV in tension can be calculated as a function of the initial temperature T_0 . Such calculations have been reported in [17] for Cu and Al, the results are reproduced in Fig. 6. As expected, due to the thermal

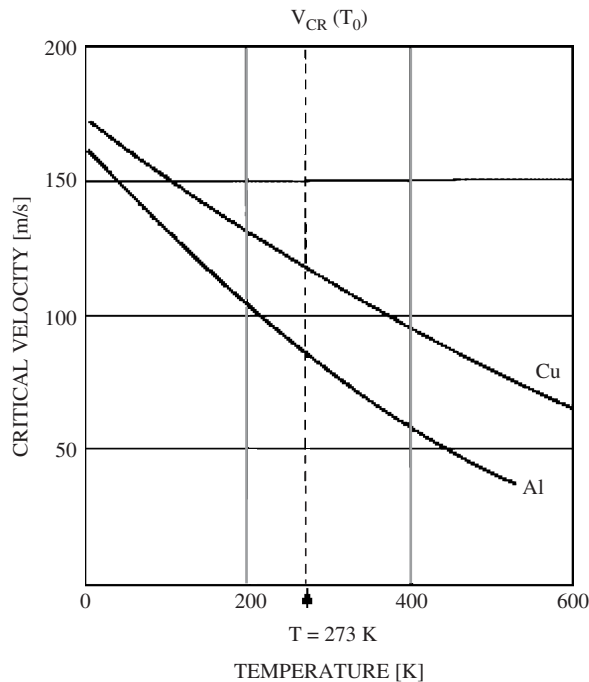


Fig. 6. Calculated values of the CIV in tension for Al and Cu as a function of the initial temperature [17].

softening, the CIV diminishes when the initial temperature is increased. The decrease is almost linear versus temperature. At room temperature values of the CIV are, respectively for Al and Cu, are 80 m/s and 113 m/s. Comparison with experiments indicates that for the polycrystalline aluminum and its alloys in the annealed state the CIV varies between 60 and 70 m/s as compared with value 80 m/s resulting from theoretical estimation. For polycrystalline copper in the annealed state the experimental values vary between 60 and 80.5 m/s as compared with 113 m/s from theoretical analysis. It is presumed that higher theoretical values than those obtained from experiment are due to lack of taking into account the thermal coupling in the form of adiabatic heating. This fundamental problem is discussed in the further part of this paper. In conclusion, theoretical estimation of the CIV with the initial temperature T_0 as a parameter can be understood as the first approximation. In such case the CIV is given by

$$v_{cr}(T_0) = C_0(0) \left\{ 1 - \frac{T_0}{T_m} \exp \left[\theta * \left(1 - \frac{T_m}{T_0} \right) \right] \right\}^{1/2} \varepsilon_e + \left[\frac{1}{\rho(T_0)} f_2(\dot{\varepsilon}) f_3(T_0) \right]^{1/2} \int_{\varepsilon_e}^{\varepsilon_{pm}} \left(\frac{df_1}{d\varepsilon_p} \right)^{1/2} d\varepsilon_p. \quad (17)$$

It is possible to calculate numerically the CIV as a function of the initial temperature T_0 when explicit forms of f_1 , f_2 and f_3 are known. In general, the positive rate sensitivity causes that $f_2(\dot{\varepsilon})$ is an increasing function of strain rate. It is shown however in Figs. 4 and 5 that is sufficient to assume f_2 as a constant multiplication factor say, for strain rate $\sim 5 \times 10^2 \text{ s}^{-1}$. Although the explicit solution for the CIV has been derived, Eq. (17), the problem arises how to determine the upper limit ε_m of the integral. The procedure of ε_m derivation is outlined later on when the shear mode of deformation is analyzed. The instability condition in the adiabatic case is applied in that case:

$$(d\sigma/d\varepsilon)_{\text{adiabatic}} = 0 \text{ at constant strain rate.}$$

In order to illustrate quantitative changes of the CIV a simple explicit form of the constitutive relation has been assumed in the following form:

$$\sigma(\varepsilon_p, \dot{\varepsilon}, T) = B \varepsilon_p^n f_2(\dot{\varepsilon}) \left(1 - \frac{T}{T_m} \right), \quad (18)$$

where T_m is the melting point. The strain hardening in Eq. (18) are assumed in the power form n and the thermal softening is assumed as linearly decreasing function of the homologous temperature. The effect of temperature on elastic constants is neglected. In order to integrate Eq. (17) the upper limit of integration is assumed in the form of Considère's condition, that is $\varepsilon_m = n$. After integration the CIV is given by

$$v_{cr}(n, T_0) = C_0(T_0) \varepsilon_e + \left[\frac{1}{\rho} f_2(\dot{\varepsilon}) \left(1 - \frac{T_0}{T_m} \right) \right]^{1/2} \frac{2\sqrt{nB}}{n+1} (n^{(n+1)/2} - \varepsilon_e^{(n+1)/2}). \quad (19)$$

The numerical analysis of Eq. (19) was focused on the effect of strain hardening and the initial temperature on the CIV. The constants in Eq. (18) are assumed to be for a mild steel, $\varepsilon_e = 10^{-3}$, $\rho = 7.8 \text{ g/cm}^3$, $B = 500 \text{ MPa}$, $T_m = 1800 \text{ K}$, $f_2 = 1.0$, $E_0 = 220 \text{ GPa}$, $C_0(300) = 5.0 \text{ mm}/\mu\text{s}$. The range of the absolute temperature $0 < T_0 < 500 \text{ K}$, and the range of the strain hardening exponent $0 < n < 0.5$. The results of the numerical calculations are shown in the form of $v_{cr}(n, T_0)$ in Fig. 7. The first conclusion can be drawn that the strain hardening rate is very important, the CIV increases almost linearly with n . Of course, for $\varepsilon_p = 0$ the main contribution to the CIV close to $\sim 5.0 \text{ m/s}$ is the elastic term in Eq. (19).

The effect of the initial temperature on the CIV is not so large in that case. This is due to the simplified linear softening of the stress and small changes of the Young's modulus at relatively low temperatures, they are simply neglected. As discussed above the results of more exact calculations of the CIV at different initial temperatures for aluminum and copper is shown in Fig. 6. In that case the effect of temperature is almost linear. For steels there is a stress plateau within the range of temperatures from ~ 250 to $\sim 500 \text{ K}$ with a very weak temperature effect and the linear approximation is to some extent justified. At low temperatures the effect of temperature for steels on the flow stress is substantial due to thermal activation (Peierls stress [20]). This is why the numerical analyses have only a qualitative character. In order to perform more exact analyses of the CIV in tension the thermal coupling must be taken into consideration. Thermal softening during plastic deformation changes the process of plastic wave propagation, the waves are slower and the instability strain appears earlier.

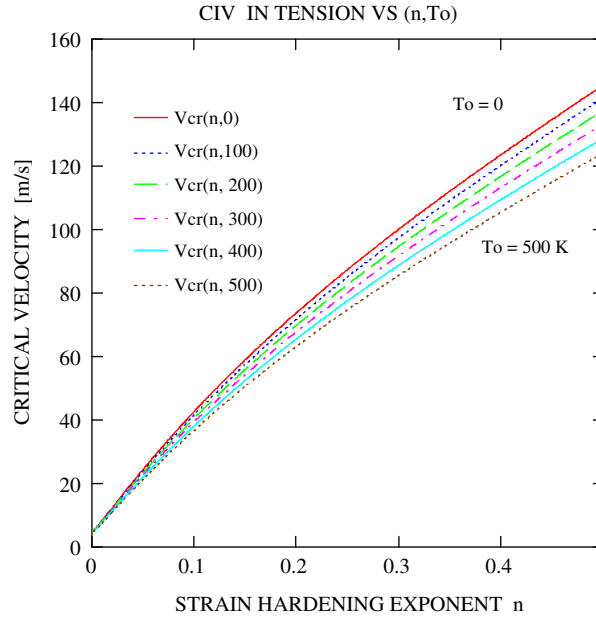


Fig. 7. Calculated values of the CIV in tension versus strain hardening exponent n , Eq. (19), for different initial temperatures T_0 , $0\text{ K} < T_0 < 500\text{ K}$.

6. Wave propagation in adiabatic conditions—complete thermal coupling

In the previous analysis of the CIV in tension the adiabatic heating was neglected. A more complete, and closer to the reality of fast plastic deformation, is assumption of the adiabatic deformation. In general, plastic waves are in its nature *adiabatic*, that means that large part of the energy of plastic deformation carried by the wave is converted into heat. Thermal softening diminishes the rate of strain hardening and plastic waves slow down. In addition, adiabatic heating accelerates plastic instabilities, for example adiabatic necking or adiabatic shear bands. The equation of energy balance with conduction and internal heat sources applicable to dynamic plasticity is given by

$$\rho(T)Q_p(T) \frac{\partial T}{\partial t} = \beta\sigma(\varepsilon_p, \dot{\varepsilon}, T) \frac{\partial \varepsilon_p}{\partial t} - \lambda(T) \frac{\partial^2 T}{\partial x_1^2}, \tag{20}$$

where ρ , Q_p , β and λ are, respectively, the density, the specific heat, Taylor–Quinney coefficient and the thermal conductivity (Fourier constant). The coefficient β defines the part of the mechanical energy converted into heat, typical value $\beta \approx 0.9$, ε_p and σ are, respectively, the plastic strain and true stress. The direction of the heat conduction is x_1 . If the adiabatic process of deformation dominates then there is no time for the heat conduction and $\lambda \approx 0$. The problem reduces to the first order ordinary differential equation

$$\frac{dT}{d\varepsilon_p} = \frac{\beta}{\rho(T)Q_p(T)} \sigma(\varepsilon_p, \dot{\varepsilon}, T). \tag{21}$$

Further simplification is possible assuming $\rho(T) = \text{const}$ and $Q_p(T) = \text{const}$. It is known that in the range of very low temperatures the specific heat Q_p is a strong function of temperature, Debye or Einstein model, but at temperatures higher than the Debye temperature a constant value is acceptable. Integration of Eq. (21) can be done with the initial conditions: $T = T_0$ for $\varepsilon_p = 0$, then

$$\Delta T_A \approx \frac{\beta}{\rho Q_p} \int_0^{\varepsilon_{pm}} \sigma[\varepsilon_p, T(\varepsilon_p), \dot{\varepsilon}] d\varepsilon_p, \tag{22}$$

where $\Delta T_A = T - T_0$ is the adiabatic increment of temperature.

Since it is stated that the plastic waves are in its nature adiabatic, and remembering that the strain rate in the wave front may vary from $\sim 10^2 \text{ s}^{-1}$ to $\sim 5 \times 10^2 \text{ s}^{-1}$, it would be important to evaluate transition from the isothermal to the adiabatic conditions versus strain rate. The numerical analyses on that subject were reported in [21]. The mean transition from the isothermal to the adiabatic process of deformation occurs within one decimal order of strain rate. The mean factors in strain rate transition are the thermal conductivity (Fourier constant) and specific heat. For example the mean values of strain rate when the transition occurs are: for a mild steel in shear $\dot{\epsilon}_{tr} \approx 60 \text{ s}^{-1}$, for aluminum $\dot{\epsilon}_{tr} \approx 89 \text{ s}^{-1}$ and for copper $\dot{\epsilon}_{tr} \approx 112 \text{ s}^{-1}$. All values of the transition strain rate cited here indicate that plastic waves in metals and alloys are indeed *adiabatic* in its nature.

Preliminary analysis of plastic wave propagation in adiabatic conditions was reported in [19]. It was shown that due to heat generated by plastic deformation and thermal softening the speed of plastic waves is reduced in comparison to the isothermal case. In order to find the “adiabatic” wave speed the “adiabatic” tangent modulus $(d\sigma/d\epsilon)_A$ must be determined. The wave speed, Eq. (7), is modified to

$$C_p(\epsilon_p) = \pm \left(\frac{1}{\rho(T)} \left(\frac{d\sigma}{d\epsilon_p} \right)_A \right)_{\dot{\epsilon}, T}^{1/2}. \tag{23}$$

If constitutive relation of the multiplicative form, Eq. (15), is applied then the wave speed is given by

$$C_p(\epsilon_p)_{A, \dot{\epsilon}} = \pm \left\{ \frac{1}{\rho(T)} f_2(\dot{\epsilon}) \frac{d}{d\epsilon_p} [f_1(\epsilon_p) f_3(T(\epsilon_p))] \right\}_{\dot{\epsilon}, T}^{1/2}. \tag{24}$$

In the simplified notation

$$C_p(\epsilon_p)_{A, \dot{\epsilon}} = \pm \left\{ \frac{1}{\rho(T)} f_2 \left[\frac{df_1}{d\epsilon_p} f_{3A} + f_1 \frac{df_{3A}}{d\epsilon_p} \right] \right\}_{\dot{\epsilon}, T}^{1/2}, \tag{25}$$

where f_{3A} accounts also for the temperature increase as a function of plastic strain during adiabatic heating. Eq. (25) can be transformed into the following form:

$$C_p(\epsilon_p)_{A, \dot{\epsilon}} = \pm \left\{ \frac{1}{\rho(T)} f_2 f_{3A} \frac{df_1}{d\epsilon_p} \left[1 + \frac{f_1}{df_1/d\epsilon_p} \frac{df_{3A}/d\epsilon_p}{f_{3A}} \right] \right\}_{\dot{\epsilon}, T}^{1/2}. \tag{26}$$

Since the first term in Eq. (26) is always positive, the second term in the case of thermal softening defines the critical plastic strain when the wave speed becomes *zero*. This happens because the derivative $df_{3A}/d\epsilon_p$ which defines the effect of temperature on the flow stress is normally *negative*. In general, if a thermal softening is present and $df_{3A}/d\epsilon_p$ is *negative* then the speed of the adiabatic waves is always lower than in the isothermal case, thus $C_p(\epsilon_p)_A \leq C_p(\epsilon_p)_T$. In Eq. (26) the function $f_3(T(\epsilon_p)_A)$ must be determined, where $T(\epsilon_p)_A$ is the evolution of temperature during adiabatic heating. Then combination of Eqs. (15) and (21) yields

$$\left(\frac{dT}{d\epsilon_p} \right)_{A, \dot{\epsilon}} = \frac{\beta}{\rho(T) Q_p(T)} f_1(\epsilon_p) f_2(\dot{\epsilon}) f_3(T(\epsilon_p)_A). \tag{27}$$

This time the integration is more complicated because in f_3 the adiabatic evolution of temperature $T(\epsilon_p)_A$ is embedded, thus

$$\int \frac{dT}{f_3(T)} = \frac{\beta}{\rho(T) Q_p(T)} f_2(\dot{\epsilon}) \int f_1(\epsilon_p) d\epsilon_p + A. \tag{28}$$

In order to obtain the adiabatic history of temperature $T(\epsilon_p)_A$, Eq. (28) must be solved with the initial conditions $T = T_0$ when $\epsilon_p = 0$.

Numerical calculations have been performed with the simplified constitutive relation, Eq. (18). The main target was to demonstrate differences in isothermal and adiabatic speed of plastic waves. Identification of all three functions f_1 , f_2 and f_3 gives the following result:

$$f_1(\epsilon_p) = B\epsilon_p, \quad \frac{df_1}{d\epsilon_p} = \frac{nB}{\epsilon_p^{1-n}}, \quad f_2(\dot{\epsilon}) = 1, \quad f_3(T) = 1 - \frac{T}{T_m}. \tag{29}$$

After substitution of the set (29) into Eq. (28) and integration one yields the adiabatic evolution of temperature in the following form:

$$T(\varepsilon_p)_A = T_m \left[1 - \left(1 - \frac{T_0}{T_m} \right) \exp\left(\frac{b}{n+1} \varepsilon_p^{n+1} \right) \right] \quad \text{with the constant } b = \frac{\beta B}{\rho Q_p} \frac{1}{T_m} \quad (30)$$

and

$$f_3(T(\varepsilon_p)_A) = \left(1 - \frac{T_0}{T_m} \right) \exp\left(-\frac{b}{n+1} \varepsilon_p^{n+1} \right). \quad (31)$$

In addition

$$\frac{df_{3A}}{d\varepsilon_p} = -b \left(1 - \frac{T_0}{T_m} \right) \varepsilon_p \exp\left(-\frac{b}{n+1} \varepsilon_p^{n+1} \right). \quad (32)$$

Value of constant b is $b = 6.41 \times 10^{-2}$, $Q_p(300) = 500 \text{ J/kg K}$ and $\beta = 0.9$. In order to compare $C(\varepsilon_p)_A$ with $C(\varepsilon_p)_T$ the velocity of isothermal plastic waves must be determined. By application of Eq. (16) and Eq. (29) one obtains the expression for the isothermal plastic wave speed

$$C(\varepsilon_p)_A = \pm \left[\frac{B}{\rho} \left(1 - \frac{T_0}{T_m} \right) \frac{n}{\varepsilon_p^{1-n}} \right]^{1/2}. \quad (33)$$

The result of calculation, in order to illustrate how the isothermal wave speed changes versus plastic strain at different strain hardening exponent, is shown in Fig. 8. Of course, the speed increases when the strain hardening is more intense. However, the values at strains larger than ~ 0.2 are very low in comparison to the elastic wave speed in slender bars, $C_0 = 5 \times 10^3 \text{ m/s}$. With the power strain hardening the wave speed reaches zero at infinite strain. This illustrates that in that case a cutoff condition of integration must be applied in determination of CIV, for example the Considère condition. In the adiabatic case, due to the thermal softening, the wave speed diminishes naturally to zero at specific plastic strain. In order to show differences between isothermal and adiabatic wave speeds Eq. (26) together with relations (29)–(32) have been combined. The simplified constitutive relation was applied and the result is given by

$$C(\varepsilon_p)_A = \pm \left[\frac{B}{\rho} \varepsilon_p^n \left(1 - \frac{T_0}{T_m} \right) \left(\frac{n}{\varepsilon_p} - b\varepsilon_p \right) \exp\left(-\frac{b}{n+1} \varepsilon_p^{n+1} \right) \right]^{1/2}. \quad (34)$$

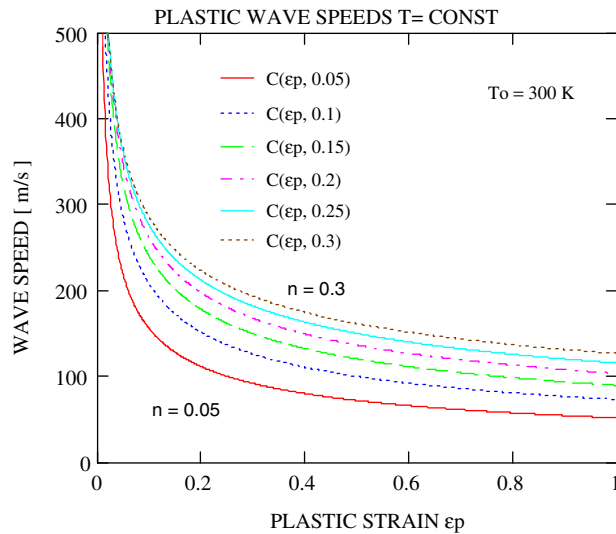


Fig. 8. Calculated isothermal speeds of plastic waves for different strain hardening exponents from 0.05 to 0.3 versus plastic strain.

Due to the third term in Eq. (34) the wave speed reaches zero at the critical plastic strain ϵ_{pc} . This condition can be found assuming that this term is zero, the solution is

$$\epsilon_{pc} = \left(\frac{n}{b}\right)^{1/2} \quad \text{or with constant } b \quad \epsilon_{pc} = \left(\frac{nB\beta f_2(\dot{\epsilon})}{\rho Q_p T_m}\right)^{1/2}. \quad (35)$$

This is interesting result which indicates that the critical plastic strain is a function of physical parameters like strain hardening and physical constants. The symbolic effect of the strain rate sensitivity is retained in Eq. (35). A positive rate sensitivity increases the critical strain, in the numerical calculations $f_2 = 1$. For the parameters assumed in the calculations the constant $b = 6.41 \times 10^{-2}$ and Eq. (35) reduces to $\epsilon_{pc} = 3.9498 (n)^{1/2}$. The critical strain ϵ_{pc} is plotted versus the strain hardening exponent n in Fig. 9. It is clear, this preliminary result indicates a very steep increase of the critical strain for small values of n . A realistic value of n for a mild steel is ~ 0.2 and for this value of n the critical plastic strain is ~ 1.75 and there is a high probability that the neck will occur earlier. Because both parameters, that is the critical strain in the adiabatic conditions ϵ_{cr} and the strain of necking $\epsilon_n = n$ are the upper limits of integration in determination of the CIV in tension the CIV calculated with the Considère condition will be lower than that determined by the critical strain obtained via adiabatic deformation. The straight line in Fig. 9 represents the condition $\epsilon_n = n$.

The wave speeds in the adiabatic conditions were calculated according Eq. (34), they are shown in Figs. 10a,b and c. Fig. 10a is for larger values of n , from 0.05 to 0.3 ($n = 0.05; 0.1; 0.15; 0.2; 0.25$ and 0.3 , Fig. 10b is limited to smaller n ($n = 0.01; 0.02; 0.03; 0.04$ and 0.05 , finally Fig. 10c shows the wave speeds for lower range of n ($n = 0.0005; 0.001; 0.002$ and 0.003). This is practically the range of the ideal plasticity and accordingly the critical strains are relatively small, less than 0.2. Finally, comparison of the isothermal and adiabatic wave speeds for $n = 0.01$ and 0.05 is shown in Fig. 11, the curves denoted T and A are, respectively, for the isothermal and adiabatic conditions. The differences are substantial for larger deformations. All calculations and figures indicate that the whole analysis is quantitatively correct. Because variables, parameters and constants are assumed as approximate, mainly due to the simplified constitutive relation, all analyses are, of course, preliminary. A more exact analyses will be possible in the future, here is only shown how to deal with the problem.

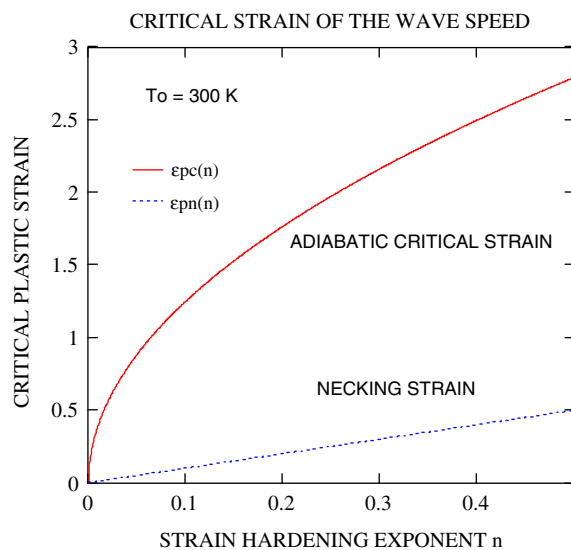


Fig. 9. Calculated critical strains for $C_{pA} = 0$ versus strain hardening exponent n , C_{pA} is the speed of plastic wave at the critical strain ϵ_{cr} in adiabatic conditions. The Considère condition $\epsilon_n = n$ is shown as the straight line.

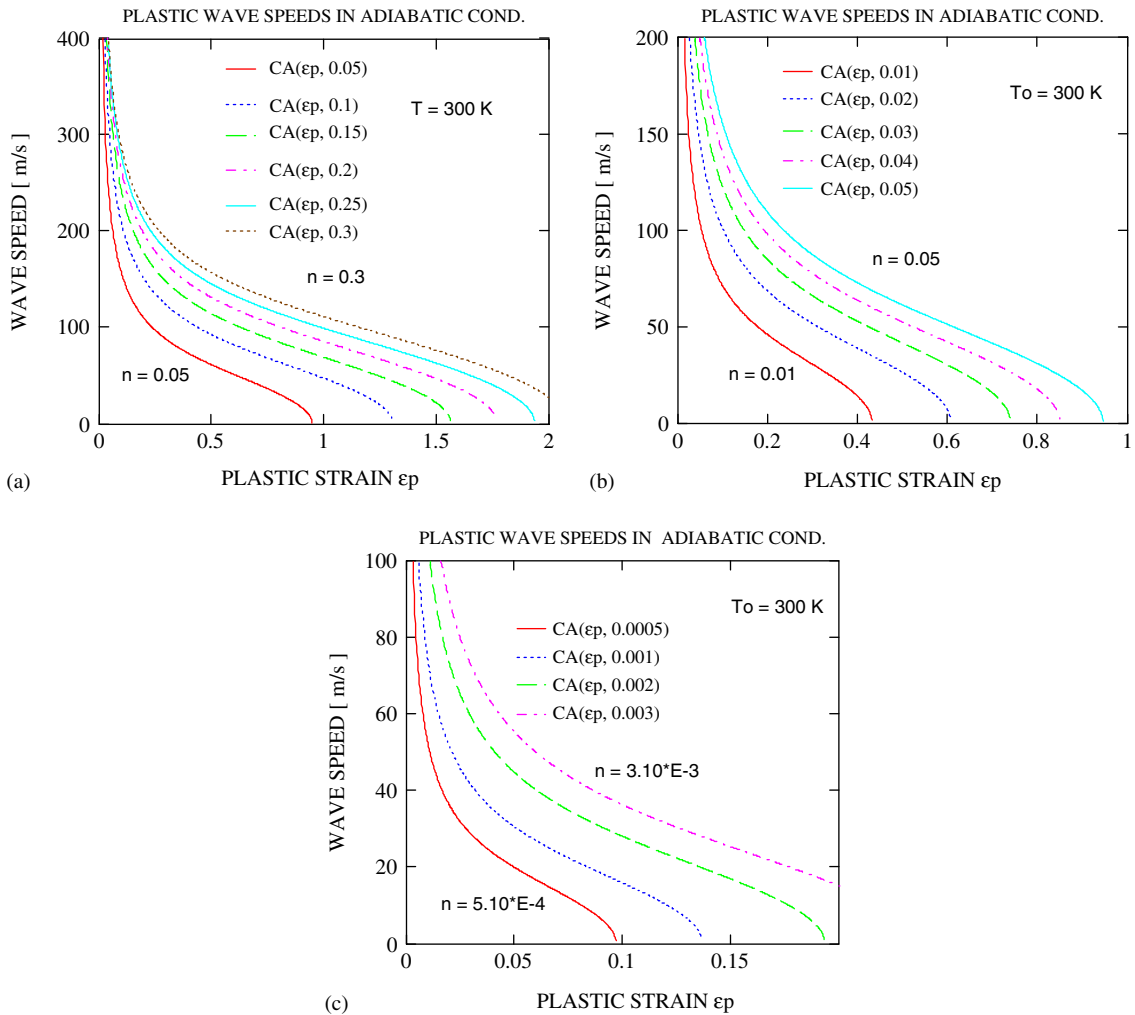


Fig. 10. Plastic wave speeds in adiabatic conditions versus plastic strain, (a)—large strains $0 < \epsilon_p < 2.0$; (b)—medium strains $0 < \epsilon_p < 1.0$; (c) small strains $0 < \epsilon_p < 0.2$.

7. The critical impact velocity in tension—complete thermal coupling

The same main conclusions as stated above can be drawn on the level of approximation in calculations of the CIV. The CIV in tension in the adiabatic conditions is obtained by introduction of Eq. (34) into Eq. (10) with the upper limit of integration $\epsilon_{cr} = (n/b)^{1/2}$. The final solution for the adiabatic CIV is given by

$$v_{cr}(\epsilon_p)_A = C_0(T_0)\epsilon_e + \left(\frac{B}{\rho}\right)^{1/2} \left(1 - \frac{T_0}{T_m}\right)^{1/2} \int_{\epsilon_e}^{\epsilon_{cr}} \left[\epsilon_p^n \left(\frac{n}{\epsilon_p} - b\epsilon_p\right) \exp\left(-\frac{b}{n+1} \epsilon_p^{n+1}\right)\right]^{1/2} d\epsilon_p. \tag{36}$$

Relation of the elastic wave speed with temperature $C_0(T)$ is given by Eq. (14). The results of the complete numerical calculations in the form of the CIV versus the strain hardening exponent n is given for $100 < T_0 < 500$ K in Fig. 12. The range of calculations is the same as for Fig. 7 where the CIV was calculated at the same initial temperatures up to 500 K applying the $\epsilon_n = n$ as the upper limit of integration. As expected this condition imposes the lower bound in estimation of CIV in tension. The upper bound is given by the condition in the form of Eq. (35). Experiments indicate that for the strain hardening exponent $n \approx 0.2$ at room temperature the CIV is much in excess of ~ 100 m/s, whereas the condition $\epsilon_n = n$ limits the CIV to ~ 60 m/s.

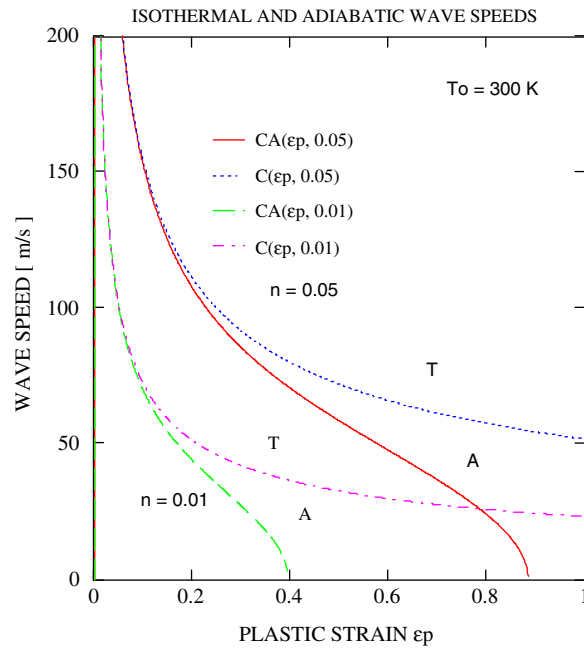


Fig. 11. Comparison of isothermal and adiabatic plastic wave speeds at $T_0 = 300$ K versus plastic strain for two values of the strain hardening exponent: $n = 0.01$ and 0.05 .

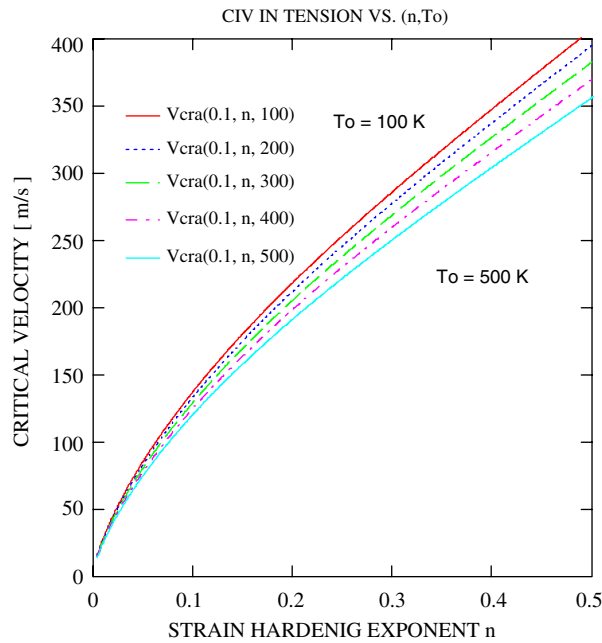


Fig. 12. Calculated values of the CIV in tension with complete thermal coupling for five initial temperatures T_0 , $100 \text{ K} < T_0 < 500 \text{ K}$, versus strain hardening exponent n .

Therefore, the condition $\epsilon_{cr} = (n/b)^{1/2}$ derived on the basis of full adiabatic coupling seems to be better as the upper limit of integration in estimation of the CIV in tension. Value of the CIV in Fig. 12 for strain 0.2 is ~ 190 m/s. Since the analysis is rather qualitative, further studies are needed on this subject, including

experiments. Experimental data are scarce, for example the CIV for 17-7 PH stainless steel and Vascojet 1000 are respectively ~ 135 and ~ 65 m/s [15]. With $n = 0.25$ the CIV in tension has been estimated numerically for a mild steel in [16]. The analysis revealed the CIV ~ 127 m/s. More recent verification of the CIV in tension for a mild steel by the finite element code (FE code Abaqus), [22], have shown the CIV around 120 m/s.

8. The Critical Impact Velocity in shear—fundamentals

Localization of plastic deformation during fast shearing by adiabatic shear band (ASB) is a common failure mode in many materials. Examples are fragmentation, armor penetration, punching, piercing, high-speed machining and others. Although the phenomenon of the ASB is known for a long time the CIV in shear has been noticed more recently. In the past the CIV in shear has not been studied extensively, but in recent years more attention is given to that problem. Early remarks on possibility of the CIV in shear can be found in [5,6]. If the rate of shearing is sufficiently high the adiabatic process of deformation is superimposed on propagation of plastic waves in shear and it leads to failure near the area of impact. The main difference of shear in comparison to tensile loading is that the cross section of the deformed area remains *constant*. Such type of deformation is met in torsion of bars and tubes and in shearing of plates and sheets. Thus, the effect of the geometrical instability like necking does not occur in shearing. The only mechanism leading to instability is the material softening due to adiabatic heating. In that way the CIV in shear can be only well defined by the material behavior. Of course, in real cases of more brittle materials there is a probability that failure in shear may occur earlier.

The theory of CIV in shear is similar to one in tension, but the main factor is the thermal coupling which must be considered. If the direction of shearing is x_1 then direction of the elastic and plastic wave propagation is x_2 . Such situation is shown in Fig. 13. A plane block is submitted to shear by velocity V in x_1 direction, the waves propagate in the direction x_2 . After initial uniform shear deformation the adiabatic shear band occurs near the surface where the velocity V is imposed. Because elastic and plastic waves propagate in x_2 direction and displacement is in x_1 direction, the wave equation is given by

$$\frac{\partial U_1}{\partial t^2} = C_2^2(\Gamma) \frac{\partial U_1}{\partial x_2}, \tag{37}$$

where U_1 is the displacement in x_1 direction. The wave speeds in the elastic and plastic range are given by

$$C_{2e} = \pm \left(\frac{\mu(T)}{\rho(T)} \right)^{1/2}, \quad C_{2p}(\Gamma_p) = \pm \left[\frac{1}{\rho(T)} \left(\frac{d\tau}{d\Gamma_p} \right) \right]^{1/2}, \tag{38}$$

where $\mu(T)$ is the temperature-dependent shear modulus, τ is the shear stress, Γ and Γ_p are respectively the shear gradients, $\Gamma = dx_1/dx_2$, total and plastic, C_{2e} is the elastic wave speed in shear and $C_{2p}(\Gamma_p)$ is the plastic wave speed. It may be mentioned that $C_2 < C_0$. The ratio $C_0/C_{2e} = (2(1 + \nu))^{1/2}$, where ν is the Poisson’s ratio, for $\nu = 1/3$ $C_0/C_2 = (8/3)^{1/2}$ and $C_0/C_{2e} = 1.633$. The same occurs for the plastic waves, the shear waves are slower. The strain amplitude of a plastic wave is constant long the nonlinear characteristics

$$\frac{dx_2}{dt} \pm C_{2p}(\Gamma_p) = 0 \quad \text{the mass velocity remains constant} \quad d \left[\int_0^{\Gamma_m} C_{2p}(\Gamma_p) d\Gamma_p \pm v \right] = 0. \tag{39}$$

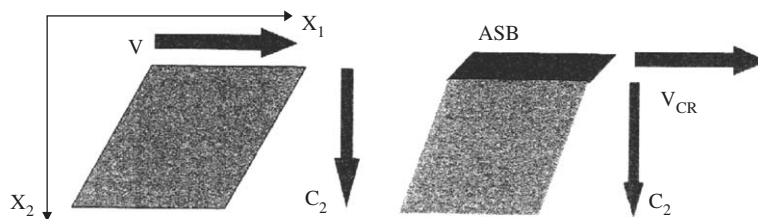


Fig. 13. Schematic representation of a block in shearing mode, V —imposed velocity, C_2 -propagation direction of elastic and plastic waves; the right side shows the critical conditions with the wave trapping by ASB.

The mass velocity in shear is given by

$$v = \pm \int_0^{\Gamma_m} C_{2p}(\Gamma_p) d\Gamma_p \quad \text{for } T = \text{const and } \dot{\epsilon} = \text{const}, \quad (40)$$

where Γ_e is the elastic shear strain at the yield limit and Γ_m is the total instability strain in the *adiabatic* conditions of deformation. In this case the upper limit of integration Γ_m is well defined as the shear strain where the adiabatic instability occurs. The instability point is defined by $(d\tau/\Gamma)_A = 0$ that occurs at Γ_m . It must be remembered that all derivations are valid for constant strain rate, characteristic for the process of plastic wave propagation, that is $5 \times 10^2 \text{ s}^{-1} < \dot{\Gamma} < 10^3 \text{ s}^{-1}$. The earliest analyses of the CIV in shear were published in [7,8]. Again, if by analogy to Eq. (15) the following constitutive relation is assumed in the case of shear:

$$\tau(\Gamma_p, \dot{\Gamma}, T) = f_1(\Gamma_p)f_2(\dot{\Gamma})f_3(T) \quad (41)$$

and the adiabatic instability condition is applied $(d\tau/\Gamma)_A = 0$, then the critical shear strain Γ_{pm} can be found. After differentiation of Eq. (41) and introduction into the instability condition the following relation is obtained

$$\left(\frac{\partial \tau}{\partial \Gamma_p}\right)_{T, \dot{\Gamma}} + \left(\frac{\partial \tau}{\partial T}\right)_{\Gamma, \dot{\Gamma}} \frac{dT}{d\Gamma_p} + \left(\frac{\partial \tau}{\partial \dot{\Gamma}}\right)_{T, \Gamma} \frac{d\dot{\Gamma}}{d\Gamma_p} = 0. \quad (42)$$

Condition (42) can be satisfied only in very specific processes of plastic deformation, one of them is adiabatic deformation at constant strain rate. Thus condition (42) reduces to

$$\left(\frac{\partial \tau}{\partial \Gamma_p}\right)_{T, \dot{\Gamma}} + \left(\frac{\partial \tau}{\partial T}\right)_{\Gamma, \dot{\Gamma}} \left(\frac{dT}{d\Gamma_p}\right)_A = 0. \quad (43)$$

Assuming constitutive relation (41) the adiabatic increase of temperature can be found after Eqs. (20) and (21). The result by analogy to Eq. (21) is given by

$$\frac{dT}{d\Gamma_p} = \frac{\beta}{\rho(T)Q_p(T)} \tau(\Gamma, \dot{\Gamma}, T). \quad (44)$$

If the explicit forms of the partial differentials derived after the constitutive relation, Eq. (41) in present case, can be found then condition (43) transforms into

$$\left(\frac{\partial f_1}{\partial \Gamma_p}\right) + f_1^2(\Gamma_{pm})f_2(\dot{\Gamma})\left(\frac{\partial f_3}{\partial T}\right) \frac{\beta}{\rho(T)Q_p(T)} = 0. \quad (45)$$

Since $f_1(\Gamma_{pm})$ depends only on the critical shear strain the non-explicit solution for $f_1(\Gamma_{pm})$ is given by

$$f_1(\Gamma_{pm}) = \left[-\frac{\rho(T)Q_p(T)}{\beta f_2(\dot{\Gamma})} \frac{(df_1/d\Gamma_p)}{(df_3/dT)_A} \right]^{1/2}, \quad (46)$$

where $(df_3/dT)_A$ is the adiabatic history of temperature. The expression $[\bullet]^{1/2}$ in Eq. (46) has real and imaginary components. Inversion of Eq. (40) enables finding of the upper limit of integration Γ_{pm} in Eq. (48). A more detailed discussion of Eq. (46) can be found in [7,8].

Finally, in general case the speed of plastic waves in shear and in adiabatic conditions is given by

$$C_{2p}(\Gamma_p, T)_{A, \dot{\epsilon}} = \pm \left\{ \frac{1}{\rho(T)} f_2(\dot{\Gamma}) f_{3A}(T) \frac{df_1(\Gamma_p)}{d\Gamma_p} \left[1 + \frac{f_1(\Gamma_p)}{df_1(\Gamma_p)/d\Gamma_p} \frac{df_{3A}(T)/d\Gamma_p}{f_{3A}(T)} \right] \right\}_{\dot{\epsilon}}^{1/2}. \quad (47)$$

Integration of Eq. (43) within the limits from Γ_e to Γ_m yields the CIV in shear, under assumption $\dot{\Gamma} = \text{const}$.

$$v_{cr}(\Gamma_m, T_0) = C_{2e}(T_0)\Gamma_e + \int_{\Gamma_e}^{\Gamma_{pm}} C_{2p}(\Gamma_p, T)_{A, \dot{\Gamma}} d\Gamma_p. \quad (48)$$

Because of analogy in derivation of the CIV in shear, in comparison to the CIV in tension, numerical qualitative analyses were not performed for the case of shear. This can be done by conversion of the

constitutive relation (18) from tension to shear by application of the Huber–Mises yield condition, $\sigma = 3^{1/2} \tau$, $\varepsilon = \Gamma/3^{1/2}$ and $\dot{\varepsilon} = \dot{\Gamma}/3^{1/2}$, then

$$\tau(\Gamma_p, \dot{\Gamma}, T) = \frac{B\Gamma_p^n}{3^{(n+1)/2}} f_2 \left(\frac{\dot{\Gamma}}{3^{1/2}} \right) \left(1 - \frac{T}{T_m} \right). \quad (49)$$

It can be shown that the CIV in shear is of the same order as for tension, however is lower in comparison to tension. Since the CIV in shear is another material constant important in fragmentation processes, further studies in the future on that subject would be valuable.

9. The Critical Impact Velocity in shear—experimental verification

Experiments performed at LPMM with the direct impact modified double shear (MDS) technique [9], confirmed existence of the CIV in shear for many metals and alloys. The experimental technique is shown schematically in Fig. 14. Here only brief description of the MDS is given. The MDS specimen with two 2.0 mm shear zone is shown on the right hand side of Fig. 14. The deformed layer initially assures the uniform deformation in shear over its gage length 2.0 mm. The MDS specimen can be loaded at different nominal strain rates with a fast servo-hydraulic universal machine or by direct impact as is shown in Fig. 14. In the case of the direct impact the MDS specimen 6 is supported by the Hopkinson tube. The impact velocities of different-length strikers of diameter 10.0 mm can be varied from 1.0 to 200 m/s. Such impact velocities assure the nominal strain rates in shear from 5×10^2 to 10^5 s^{-1} . The impact velocity is measured by a set of three light sources 1, three photodiodes 3 and two time counters 2. The transmitted wave is measured by two SR gages 7 cemented on the surface of the Hopkinson tube. The displacement of the central part of the MDS specimen is

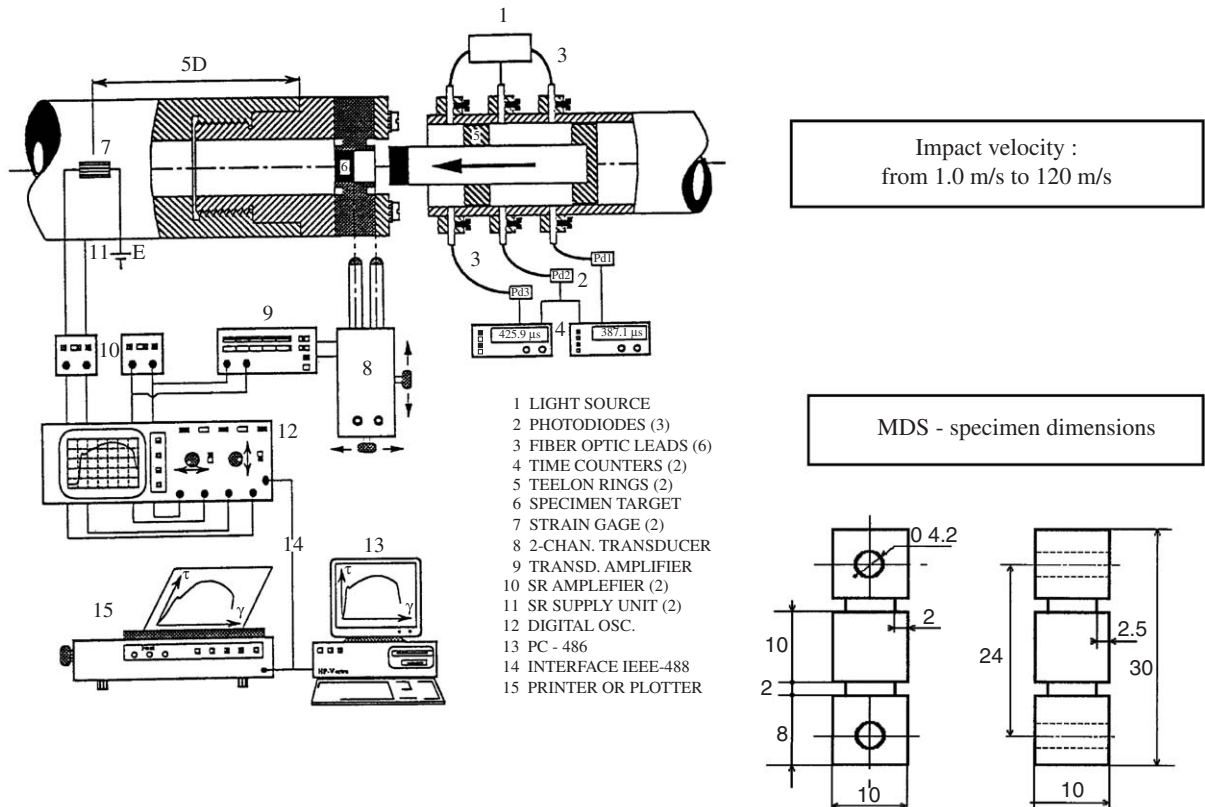


Fig. 14. Scheme of experimental arrangement for direct impact on the modified double shear (MDS) specimen shown on the right side; explanation in the text and in [9].

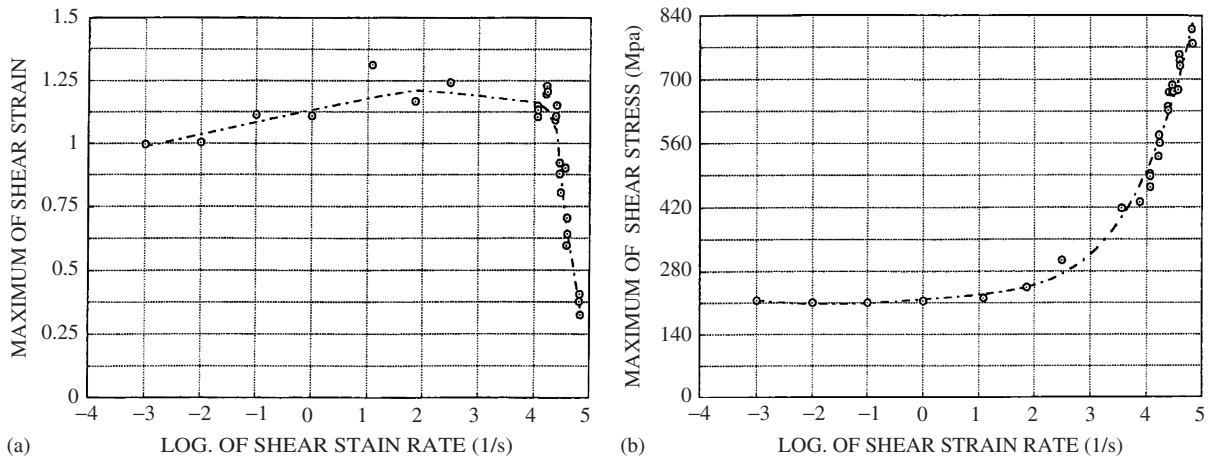


Fig. 15. Experimental results of slow and fast shearing for a hot rolled armor steel by the MDS technique: a—maximum shear strain at failure versus nominal strain rate; b—maximum shear stress versus nominal strain rate [10].

measured by the non-contact optical transducer 8 and by the black and white target 6. In addition, since the front of the striker is black the displacement of the contact striker-specimen can be also measured. The theory of the test is given in [9].

After analysis of the recorded signals and elimination of time, the force–displacement curve can be obtained and later on $\tau(\Gamma)$ and $d\Gamma/dt$ calculated. It was immediately found during preliminary tests that above shear strain rate $\sim 4 \times 10^4 \text{ s}^{-1}$ plastic shear waves obscure a correct determination of the material characteristics. When the impact velocity was increased the CIV in shear appeared. One of many results is given in Fig. 15 for hot-rolled armor steel. For this steel the CIV is estimated as ~ 60 to 80 m/s. This relatively low CIV may be attributed to plastic pre-deformation during rolling. It may be noted that the CIV is a decreasing function of pre-deformation [7]. On the other hand comparison of Fig. 15a and b indicates that in spite of decreasing of the shear strain (and the energy to failure) the maximum of stress increases. Near the CIV the apparent $\tau(\Gamma)$ curve is reduced to an intense peak. For harder steels with a proper thermal treatment the CIV can be quite high. For example, the CIV has also been experimentally determined for VAR 4340 steel (~ 52 HRC) as ~ 140 m/s [10]. Although experimental data are limited to several materials the CIV in shear has been confirmed.

10. Numerical analyses the Critical Impact Velocity in shear

Numerical analyses by FE with complete elastic and plastic wave propagation and thermal coupling also have confirmed existence of CIV in shear for VAR 4340 steel and Ti–6Al–4V alloy, [23,24].

In this paper a review and synthesis of those results are discussed. In both cases numerical studies have been performed of impact shearing of an infinite layer with the height 2.0 mm and a small geometric imperfection ($\sim 1.0\%$ of the cross section in the center) by FE code Abaqus. The constitutive relation was in an advanced form with strain hardening, strain rate sensitivity and thermal softening. The mesh applied in those calculations and the displacement fields for velocities 40 m/s ($2 \times 10^4 \text{ s}^{-1}$) and 130 m/s ($6.5 \times 10^4 \text{ s}^{-1}$) are shown in Fig. 16. At lower strain rate plastic deformation is concentrated in the middle of the shear zone, whereas at high velocity the CIV in shear is reached and in spite of the geometrical imperfection a strong plastic field is concentrated near the external cross section where the velocity is imposed. This transition is much better illustrated in Fig. 17 where the Marciniak plots in the form Γ_A (Γ_B) are shown, respectively, for velocities 40 and 115 m/s in Figs. 17a and b. The section A is in the middle of the sheared layer and section B in the upper extremity where velocity is applied. A complete inversion of the deformation history of the cross sections A and B is found when the imposed velocity was increased from 40 to 115 m/s. The standard Marciniak plot, typical for all plastic instabilities, is obtained for 40 m/s, but for 115 m/s section B deforms more rapidly indicating the first stage of the CIV process via formation of ASB and superposition of plastic waves, Fig. 13.

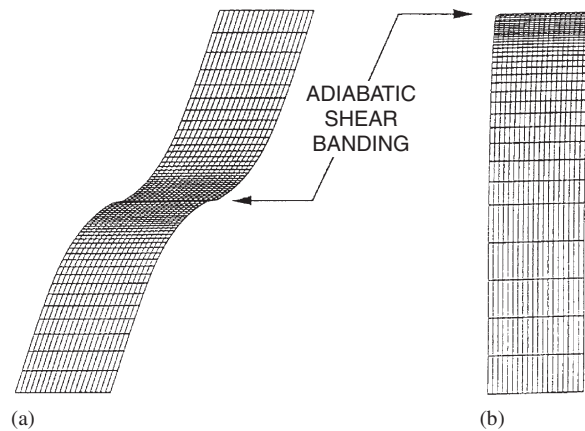


Fig. 16. Deformed FE mesh submitted to shear for imposed velocities at the top of the layer; a—low velocity case, $V = 40$ m/s, shear band occurs in the middle where a small imperfection is assumed; b—high velocity loading, $V = 130$ m/s, in spite of the imperfection in the middle ASB is triggered at the top, the CIV in shear is reached [23].

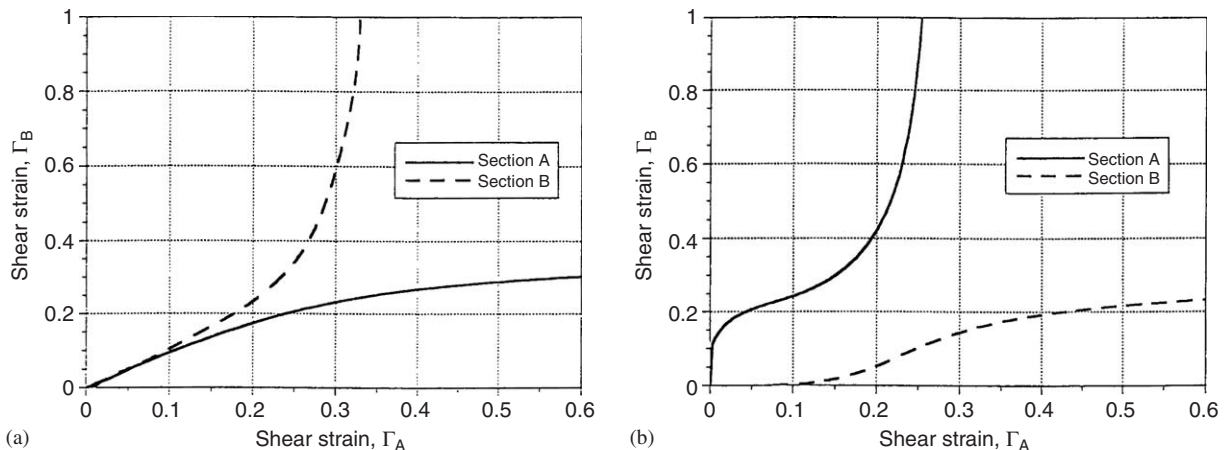


Fig. 17. Marciniaik plots Γ_A (Γ_B), the position of points A and B is shown in Fig. 16; a—imposed velocity $V = 40$ m/s, normal evolution of strains in zones A and B; b—imposed velocity $V = 130$ m/s, inversed evolution of strains in sections A and B, the CIV in shear is reached [23].

During the numerical study reported in [23] variations of the nominal shear strains at the instability point, $(d\tau/d\Gamma) = 0$, along with shear strain of the final localization (assumed in the code) were evaluated numerically as a function of the impact velocity. The result is shown in Fig. 18. Complete confirmation of the CIV is obtained not only by this figure but also by Figs. 16 and 17. Theoretical evaluation of the CIV for VAR 4340 steel indicates an almost equal contributions of the elastic and plastic terms in Eq. (44), $v_{ce} = 51.1$ and $v_{cp} = 57.0$ m/s, thus $v_c = 108.1$ m/s. The last important finding is shown in Fig. 19 where the total energy up to shear failure, independently where it may occur in the sheared layer, is shown as a function of the impact velocity. This figure explains important fact in dynamic fragmentation, namely when the shearing velocity of the material exceeds locally the CIV fragmentation can occur instantaneously.

Similar numerical results were obtained in [24] for titanium alloy Ti-6Al-4V. The nominal shear strains of instability Γ_{nc} and final localization Γ_{nl} determined numerically by FE code are shown in Fig. 20 versus impact velocity. The CIV estimation leads to ~ 132 m/s. The energy dissipated to the shear strain of localization is shown in Fig. 21. As expected, a substantial drop of the energy occurs near the CIV. Within the first region the energy to “failure” increases up to $W = 624$ MJ/m³ at $v_{cr} = 130$ m/s and next, in the transition region, a considerable decrease occurs. For impact velocity $V = 180$ m/s the energy reaches level ~ 110 MJ/m³. For

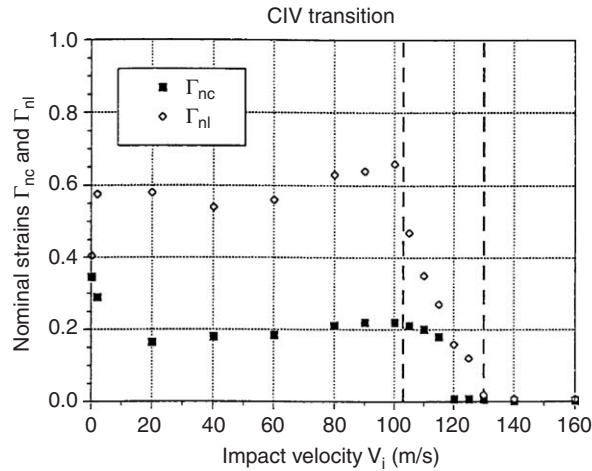


Fig. 18. Nominal shear strains of instability Γ_{nc} and advanced localization Γ_{nl} found numerically for VAR 4340 (52 HRC) steel at different velocities V , the CIV has been confirmed numerically [23].

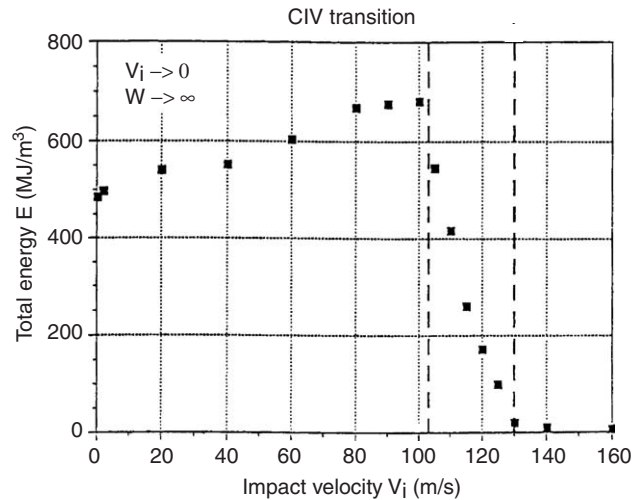


Fig. 19. Evolution of energy calculated numerically for VAR 4340 steel (52 HRC) by FE at localization strain for different velocities, the CIV in shear is confirmed. A substantial drop of the “failure energy” is observed within the CIV transition [23].

higher impact velocities the energy level practically rests constant. The energy drop is about six times when the impact velocity changes from 130 to 180 m/s. Such behavior has far reaching consequences in fragmentation. Theoretical evaluation of the CIV shows that the contribution of the elastic term $v_{ce} = 106.4$ m/s is much higher than the contribution due to plasticity $v_{cp} = 14.0$ m/s. Thus theoretical value of the CIV is 121 m/s as compared with the FE analysis $v_{cr} = 132$ m/s. Experiments and numerical analyses indicate that there is a transition of instability and localization strains, as well as the energy, when the impact velocity is increased. More exactly, the CIV can be defined as the process involving thermo-visco-plastic behavior of materials.

11. Conclusions

Existence of the Critical Impact Velocities in tension and shear has been confirmed by theoretical, experimental and numerical means. It was shown that physical parameters, including thermodynamic

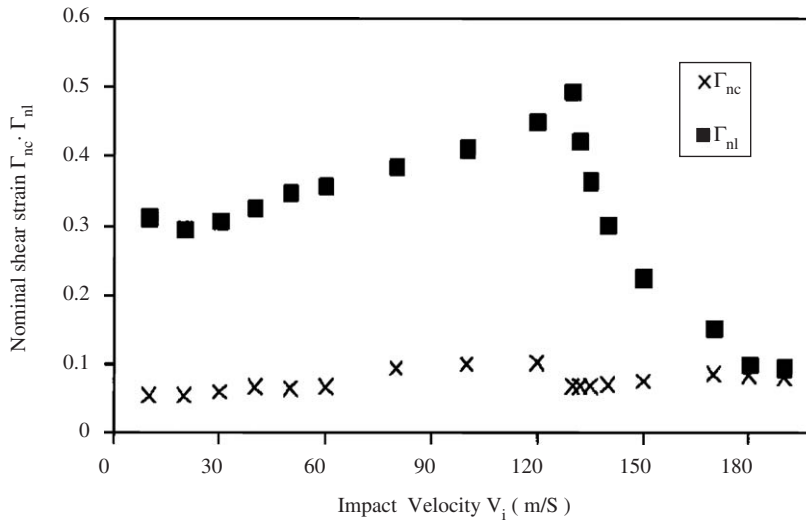


Fig. 20. Nominal shear strains at the point of instability and advanced localization determined numerically by FE for Ti–6Al–4 V titanium alloy; the CIV in shear is confirmed [24].

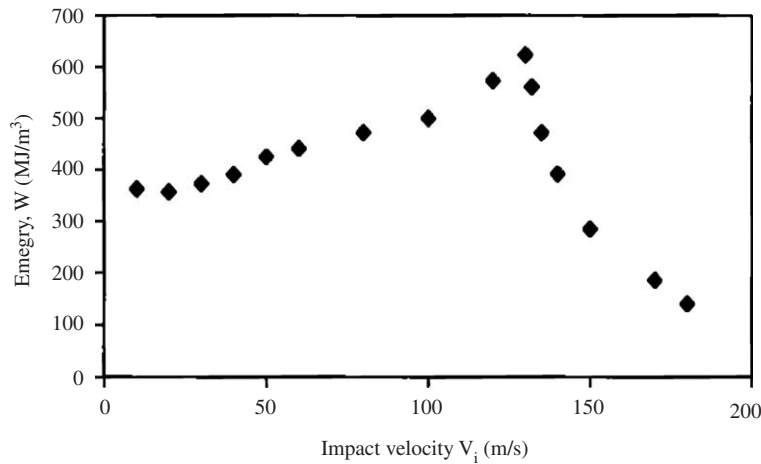


Fig. 21. Evolution of the energy to shear “failure” calculated by FE for Ti–6Al–4V versus different velocities. A substantial drop of energy is observed for this Ti alloy [24].

constants, as well as material behavior in elastic and plastic ranges are involved in estimation of the CIV. Values of the CIV, both in tension and shear, can be understood as material constants.

The CIV in tension imposes very strict limits on impact tensile testing of materials. This limitation is observed because well before occurrence of the CIV at much lower velocities the strain gradients along specimen obscure the assumption of the uniformity of the strain along specimen. The CIV in tension is the upper limit of tension impact testing. For example assuming $v_{cr} = 100$ m/s the nominal strain rate for 40 mm long specimen is 2.5×10^3 s⁻¹. Typical solution is specimen miniaturization which involves another problems not discussed here, for example the end effects in the form of stress concentrators. In general the specimen geometry for dynamic tension test must be optimized.

Theoretical analysis of the CIV in tension has been improved by introduction of complete thermal coupling in the form of adiabatic heating which slows down plastic waves leading to the natural limit $C_p = 0$, where C_p is the velocity of plastic waves. There is still unresolved question as to application of Considère condition as the upper limit of integration in Eq. (11). Further experiments should resolve this question.

Because the CIV in shear is a new material constant it can characterize resistance to dynamic fragmentation of metals and alloys, which possess some plasticity, via appearance of adiabatic shear bands (ASB). Of course, for harder materials the situation is more complex. The phenomenon of CIV in shear is relatively new. A complete analysis of the CIV in shear with thermal coupling has been performed, that is the adiabatic process of deformation superimposed on trapping of plastic shear waves was considered. It was found that a unique superposition of plastic shear waves and adiabatic softening triggers this phenomenon. Review of existing experimental results on CIV in shear, and so far reported numerical estimations, have provided a sound basis for this phenomenon. Theoretical estimations are in general in agreement with experiment and FE calculations.

It is expected that the CIV in shear is lower than that in tension. In order to establish a bank of data, for both the CIV in tension and shear, further *quantitative* analyses would be of great assets in order to create a bank of data. Comparison of data for different metals and alloys could provide better understanding which construction materials are more resistant to plastic failure under impact and fragmentation.

Acknowledgement

The research reported herein has been sponsored in part by CNRS-France and in part by the US Army through its European Research Office during last several years. Participation of the former Ph.D. students in FE numerical calculations: A.S. Bonnet-Lebouvier and M. Klosak is also acknowledged.

References

- [1] Kármán T. On the propagation of plastic deformation in solids. NDRC Report No. A-29, February 2, 1942.
- [2] Duwez PE, Clark DS. An experimental study of the propagation of plastic deformation under conditions of longitudinal impact. Proc ASTM 1947;47:502.
- [3] Taylor GI. Plastic wave in a wire extended by an impact load. Scientific papers, vol. 1 mechanics of solids. Cambridge: Cambridge University Press; 1958. p. 456.
- [4] Kármán T, Duwez P. The propagation of plastic deformation in solids. J Appl Phys 1950;21:987.
- [5] Erlich DC, Curran DR, Seaman L. Further development of a computational shear band model. SRI Report AMMRC TR 80-3, 1980.
- [6] Wu FH, Freund LB. Deformation trapping due to thermoplastic instability in one-dimensional wave propagation. J Mech Phys Solids 1984;32:119.
- [7] Klepaczko JR. Plastic shearing at high and very high strain rates. Proc Conf Eurodynat J Phys 1994;IV-4:C8.
- [8] Klepaczko JR. On the critical impact velocity in plastic shearing, EXPLOMET'95. Proceedings of the International Conference on metallurgical and materials application of shock-wave and high-strain-rate phenomena. Amsterdam: Elsevier Science, 1995. p. 413.
- [9] Klepaczko JR. An experimental technique for shear testing at high and very high strain rates, the case of mild steel. Int J Impact Eng 1994;15:29–39.
- [10] Klepaczko JR. Experimental investigation of adiabatic shear banding at different impact velocities. Final Technical Report ERO of the US Army DAJA 45-90-C0052, LPMM Metz University, 1993.
- [11] Rakhmatulin HA. Mechanics of unloading waves. Prilkl Mat Meh 1945;9:91.
- [12] Levi-Civita T. Caractéristiques des systèmes différentiels et propagation des ondes. Paris: Felix Alcan; 1932.
- [13] Mann HC. High-velocity tension-impact tests. Proc ASTM 1936;36:85.
- [14] Clark DS, Wood DS. The influence of specimen dimension and shape on the results in tension impact testing. Proc ASTM 1950;50:577.
- [15] Wood WW. Experimental mechanics at velocity extremes—very high strain rates. Experimental Mechanics 1967;7(10):441.
- [16] Hu X, Daehn GS. Effect of velocity on flow localization in tension. Acta mater 1996;44:1021.
- [17] Klepaczko JR. Generalized conditions for stability in tension test. Int J Mech Sci 1968;10:297.
- [18] Considère A. Mémoire sur l'emploi du fer et de l'acier dans les constructions. Ann des Ponts et Chaussées 1885;9:574.
- [19] Klepaczko JR. An analysis of elastic–plastic wave front in a metallic bar. Mekhanika 1971;130(6):112 (in Russian).
- [20] Klepaczko JR. A general approach to rate sensitivity and constitutive modelling of FCC and BCC metals. In: Impact: effects of fast transient loadings. Rotterdam: A.A.Balkema; 1988. p. 1.
- [21] Oussouaddi O, Klepaczko JR. An analysis of transition between isothermal and adiabatic deformation for the case of torsion of a tube. Supplément au Journal de Physique III 1991;1:323.
- [22] Rusinek A, Klepaczko JR. Size effects in dynamic tension test, numerical approach. In: Proceedings of the 14th Dymat Technical Meeting, Behaviour of Materials at High Strain Rates; Numerical Modelling. Sevilla (Spain): Universidad de Sevilla, 2002. p. 169.
- [23] Klepaczko JR, Klosak M. Numerical study of the critical impact velocity in shear. Eur J Mech A/Solids 1999;18:93.
- [24] Bonnet-Lebouvier AS, Klepaczko JR. Numerical study of shear deformation in Ti–6Al–4V at medium and high strain rates. Int J Impact Eng 2002;27:755.